Environmental Science & Technology

pubs.acs.org/est

Article

Electrochemical Hydrogen Peroxide Generation and Activation Using a Dual-Cathode Flow-Through Treatment System: Enhanced Selectivity for Contaminant Removal by Electrostatic Repulsion

Yanghua Duan and David L. Sedlak*

Cite This: *Environ. Sci. Technol.* 2024, 58, 14042−14051

Read Online

ACCESS | Metrics & More | Article Recommendations | Supporting Information

ABSTRACT: To oxidize trace concentrations of organic contaminants under conditions relevant to surface- and groundwater, air-diffusion cathodes were coupled to stainless-steel cathodes that convert atmospheric O_2 into hydrogen peroxide (H_2O_2), which then was activated to produce hydroxyl radicals ($^{\cdot}OH$). By separating H_2O_2 generation from its activation and employing a flow-through electrode consisting of stainless-steel fibers, the two processes could be operated efficiently in a manner that overcame mass-transfer limitations for O_2, H_2O_2, and trace organic contaminants. The flexibility resulting from separate control of the two processes made it possible to avoid both the accumulation of excess H_2O_2 and the energy losses that take place after H_2O_2 has been depleted. The decrease in treatment efficacy occurring in the presence of natural organic matter was substantially lower than that typically observed in homogeneous advanced oxidation processes. Experiments conducted with ionized and neutral compounds indicated that electrostatic repulsion prevented negatively charged $^{\cdot}OH$ scavengers from interfering with the oxidation of neutral contaminants. Energy consumption by the dual-cathode system was lower than values reported for other technologies intended for small-scale drinking water treatment systems. The coordinated operation of these two cathodes has the potential to provide a practical, inexpensive way for point-of-use drinking water treatment.

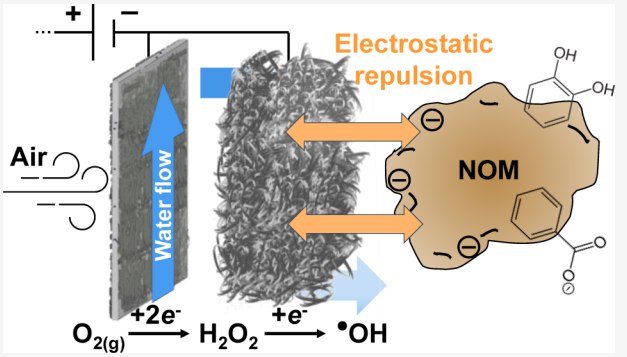

KEYWORDS: *decentralized treatment, zero-chemical-input, sequential oxygen reduction, selective transformation, coulomb repulsion*

INTRODUCTION

Advanced oxidation processes that convert H_2O_2 into $^{\cdot}OH$ have emerged as one of the main treatment technologies for removing chemical contaminants during water recycling, groundwater remediation, drinking water treatment and industrial wastewater treatment because the radicals can oxidize most contaminants without producing toxic by-products.[1,2] Despite their efficacy and popularity, advanced oxidation processes have not been used widely for small-scale treatment of nontraditional water sources due to their high costs and the logistical challenges associated with frequent replenishment of chemical reagents.

As an alternative, electrodes can be used to generate H_2O_2 via two-electron reduction of O_2. Electrodes also can convert H_2O_2 into reactive oxidants (e.g., $^{\cdot}OH$) by surface reactions with electrochemically generated reductants (e.g., Fe^{II}, H*).[3−5] Because the H_2O_2 generation and activation steps both occur on cathodes, most previous efforts to create electrochemical advanced oxidation systems use a single electrode to reduce O_2 to H_2O_2 prior to converting it into $^{\cdot}OH$.[6−15] Despite the simplicity and effectiveness of such composite cathodes under laboratory conditions, their application to actual treatment systems has been limited due to rapid consumption of dissolved O_2 which necessitates the use of pumps to introduce air or pure oxygen into the solution.[16−19] In addition, composite electrodes usually are produced as flat sheets that are subject to mass-transfer limitations. Air-diffusion electrodes offer an attractive approach for overcoming O_2 depletion problems because they passively introduce O_2 at the gas−water interface. By coupling air-diffusion electrodes with high-surface-area flow-through electrodes in a two-electrode system, it may be possible to avoid mass-transport limitations. Additionally, use of a dual-cathode system avoids inefficiencies inherent in single electrode systems in which the same potential is applied for reductive processes that have different electrochemical potentials (Text S1). As a result of this inefficiency, systems employing single composite electrodes often produce excess H_2O_2 or apply current to solutions after

Received: May 31, 2024
Revised: July 15, 2024
Accepted: July 16, 2024
Published: July 23, 2024

https://doi.org/10.1021/acs.est.4c05481
Environ. Sci. Technol. 2024, 58, 14042−14051

H_2O_2 has been depleted.[20,21] In addition to increasing energy consumption, the mismatch between H_2O_2 production and use can result in the presence of an unwanted oxidant in treated water (i.e., H_2O_2) as well as the production of other unwanted products (e.g., H_2).[22,23] Finally, electrochemical generation of H_2O_2 increases localized solution pH values, which can decrease the efficiency of H_2O_2 activation.[24]

Most previous attempts to employ separate electrodes for H_2O_2 generation and activation were simply a combination of processes that were not optimized to maximize efficiency and avoid the generation of unwanted products.[25−31] In general, prior efforts only considered contaminant transformation without measures to ensure efficient energy use or avoid excess H_2O_2 production. Furthermore, the effect of other co-occurring processes, such as the anodic decomposition of H_2O_2, were neglected because the processes were studied in batch reactors. Finally, most applications were studied under conditions that are not relevant to drinking water (e.g., pH < 3).[26,27,29−31]

Recently, a low-cost, commercially available material, stainless-steel scrubbing pads, was investigated as an electrode for converting H_2O_2 to $^{\cdot}OH$ for contaminant oxidation.[24,32] Notably, the stainless-steel electrode demonstrated higher yields for converting H_2O_2 into $^{\cdot}OH$ (i.e., ∼70%) than those typical of other anodes or heterogeneous catalysts. For example, the observed efficiency for $^{\cdot}OH$ production was over an order of magnitude higher than that reported for heterogeneous Fenton systems.[24] Although the structure of the electrode lends itself to use as a flow-through electrode, the system was only studied in a batch reactor configuration. In addition, the system was operated by externally dosing H_2O_2, which would not be suitable for distributed water treatment systems where electrochemical production via oxygen reduction would be advantageous. Finally, the performance of the electrode was not evaluated in the presence of solutes (e.g., $^{\cdot}OH$ scavengers) that could inhibit its performance, especially under low ionic strength conditions.

Finally, the efficiency of advanced oxidation processes is limited by the low selectivity of $^{\cdot}OH$, especially in the presence of natural organic matter (NOM)—a ubiquitous component of surface and groundwater that competes with contaminants for $^{\cdot}OH$.[16,24,33] In an electrochemical treatment system, the electric potential gradient can be used to separate charged species from uncharged species. The negatively charged cathode may be able to repel negatively charged NOM away from its surface and prevent its reaction with $^{\cdot}OH$ produced on the electrode surface. Despite the promise of using this approach to increase the efficiency of contaminant transformation processes, the application of electric potential gradient for selective oxidation of uncharged contaminants has not been realized.

To assess the potential for employing a dual-cathode system for efficient treatment of uncharged trace organic contaminants, we coupled an air-diffusion electrode and a flow-through stainless-steel electrode to produce $^{\cdot}OH$ from ambient air. Three reactor configurations were assessed because the interactions between electrodes could affect the H_2O_2 production and activation processes and may offer additional benefits, such as disinfection by the anodically produced free chlorine, reduced formation of disinfection products, and control of residual H_2O_2.[34] The system was optimized to ensure a proper balance between H_2O_2 production and activation under circumneutral pH conditions prior to assessing its ability to transform neutral trace organic contaminants in authentic surface waters.

MATERIALS AND METHODS

Materials. All experiments were performed at room temperature (23 ± 2 °C) with chemicals of reagent grade or higher (Sigma-Aldrich, St. Louis, MO, and Fisher Scientific, Pittsburgh, PA). Ultrapure water from a Milli-Q system (R > 18 MΩ) was used for all experiments. The composition of an authentic surface water sample tested in this study is provided in Table S1.

Electrolysis. Electrolysis experiments were conducted with a potentiostat (Gamry Instruments Inc., Warminster, PA). The internal resistance was compensated by current interrupt method. An Ag/AgCl electrode (3 M NaCl, BASi, West Lafayette, IN) was used as the reference electrode and all potentials are reported versus a standard hydrogen electrode (SHE).

The air-diffusion electrode (4 cm × 4 cm) was fabricated with carbon black (Cabot Black Pearls 2000, Cabot, Boston, MA) as the catalyst following a process described previously.[17] Because of the stable performance of the air-diffusion electrode, the same electrode was used for several experiments, encompassing a total run time of at least 90 h. The air-diffusion electrode was placed between atmospheric air and water, where the atmospheric O_2 was passively introduced to the catalyst (no air was pumped to the system). A platinized titanium (Pt/Ti) electrode (dimensions: 5.1 × 7.6 cm; TWL, United States) was used as the counter electrode for the air-diffusion electrode. Three reactor cell configurations were used to investigate the performance of the air-diffusion electrode (Figure S1): an undivided cell ($V_{effective}$ = 60 mL), a divided cell ($V_{effective,cathode}$ = 20 mL, $V_{effective,anode}$ = 30 mL), and a semidivided cell ($V_{effective}$ = 50 mL). The interelectrode distance for all cell configurations was around 2 cm. For the divided cell and semidivided cell, a cation exchange membrane (Ultrex CMI-7000, Membranes International Inc., Ringwood, NJ) was used to separate the cathode and anode chambers. The current−potential relationship of the air-diffusion cathode was evaluated in an electrolyte solution (250 mM Na_2SO_4) buffered with 50 mM of phosphate buffer at pH 7 using a divided cell configuration. Because H_2O_2 generation by the air-diffusion electrode is independent of solution composition,[16,17] the observed results represent the performance that should be encountered across a wide range of conditions.

A 20 g Scotch-Brite stainless-steel scrubber (catalogue number 214C, 3 M Company, St. Paul, MN, USA; 80 cm^2/g specific surface area) rinsed thoroughly with ultrapure water was used as the working electrode. The stainless-steel cathode was compressed into a flow-through reactor (Schedule 40 PVC, inner diameter = 3.5 cm, V = 80 mL, Figure S2) to ensure no hydraulic short-circuiting of water. A platinum (Pt) mesh counter electrode was placed about 2 mm above the stainless-steel electrode. The H_2O_2 consumption rate in the stainless-steel electrode reactor was calculated based on the concentrations of H_2O_2, recirculation rate (Q), and reaction time (T):

$$H_2O_2 \text{ consumption rate} = \frac{Q}{TV}\int_0^T ([H_2O_2]_{inf} - [H_2O_2]_{eff})dt \quad (1)$$

https://doi.org/10.1021/acs.est.4c05481
Environ. Sci. Technol. 2024, 58, 14042−14051

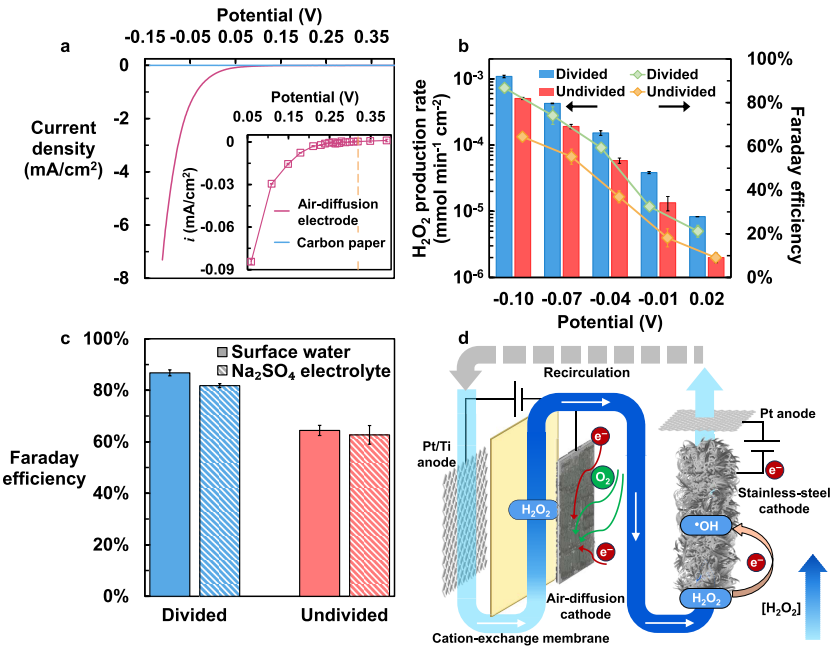

Figure 1. Production of H_2O_2 by the air-diffusion electrode. (a) Linear sweep voltammetry curves for the air-diffusion electrode and P75T carbon fiber paper substrate in 250 mM Na_2SO_4 (pH buffered at 7.0 by 50 mM phosphate buffer), potential scan rate: 2 mV s^{-1}. The inset shows the average current density observed through multiple trials (n = 4) using 5 min chronoamperometry at the specified potentials in the presence of 10 mM H_2O_2. The dashed line indicates the equilibrium potential for the H_2O_2 generation reaction in the presence of 10 mM H_2O_2 at pH 7 (E = +0.32 V). (b) H_2O_2 production rate and Faraday efficiency observed at different potentials using divided and undivided cell configurations. Experiments conducted in an authentic surface water sample amended with 250 mM of Na_2SO_4. (c) Comparison of Faraday efficiency for H_2O_2 production in surface water versus Na_2SO_4 electrolyte. Applied potential on air-diffusion electrode = −0.10 V. (d) Schematic illustration of the dual-cathode treatment system. Data are presented as mean values with standard deviation. All potentials are reported versus SHE.

The dual-cathode treatment system was evaluated by recirculating 200 mL of test solution between the two reactors. To equalize the flow of water, each reactor was equipped with a 35 mL solution reservoir. A peristaltic pump (Cole-Parmer, Chicago, IL) coupled with Norprene Tygon A-60-G tubing (Masterflex, Vernon Hills, IL) was used to circulate solution through the system. Control experiments conducted under open-circuit conditions indicated that adsorption accounted for less than 20% of the trace organic contaminants (TrOCs) loss over the 4 h experimental period (Figure S3). The same electrodes were used for replicated experiments, with no significant difference observed across replicates, indicating the stable performance of the electrodes.

Analytical Methods. Sample aliquots (<1 mL) for H_2O_2 measurement were removed from the influent and the effluent of the stainless-steel electrode. H_2O_2 was measured by the titanium(IV) sulfate method[35] or the peroxidase catalyzed N,N-diethyl-p-phenylenediamine (DPD) oxidation method.[36]

Sample aliquots (<1 mL) for other analytes were collected from the effluent of the stainless-steel electrode. Samples for TrOC analysis were quenched with methanol (final concentration = 10% v/v) and analyzed in multiple reaction monitoring mode with an Agilent 1260 series HPLC system coupled to a 6460 triple quadrupole tandem mass spectrometer (HPLC-MS/MS) as described previously.[17]

Samples containing ·OH scavengers (i.e., 2-propanol and benzoate) and their associated ·OH oxidation products (i.e., acetone, an acetone transformation product, and para-hydroxybenzoate) were analyzed on an Agilent 1260 Infinity high-performance liquid chromatography (HPLC) equipped with diode array detector (Text S2).

Aliquots for total metals analysis were acidified immediately after sampling and quantified on an Agilent 7700 Series Inductively Coupled Plasma-Mass Spectrometer (ICP-MS). Samples for TOC analysis (20 mL) were quenched by sodium thiosulfate (final concentration = 100 mM) and analyzed using a Shimadzu TOC-V analyzer.[37] COD was measured using a HACH COD kit (concentration range 3 to 150 mg/L). The interference of H_2O_2 on COD measurement was corrected based on the concentration of H_2O_2 in each sample (Figure S6).

RESULTS AND DISCUSSION

Air-Diffusion Electrode for H_2O_2 Production. The current−potential relationship can be used to match the rate of H_2O_2 production by the air-diffusion cathode to its rate of activation on the stainless-steel cathode. To develop an understanding of the process that can be used to control the rate of H_2O_2 production, the air-cathode was characterized under a range of possible operating conditions. The low onset overpotential (i.e., 30 mV, Figure 1a inset) of the air-diffusion electrode under neutral pH conditions was comparable to those reported for other catalysts capable of electrochemical H_2O_2 production (i.e., 10 to 150 mV).[38−41] The current for O_2 reduction was sensitive to the applied potential, with an increase of a factor of 10 for every 88 mV decrease in the applied potential (Figure S7).

H_2O_2 generation was assessed in two different cell configurations (Figure S1) with a sample from an authentic surface water (Figure 1b). As the applied potential decreased from +0.02 to −0.10 V vs SHE, the H_2O_2 production rate increased by a factor of 130 and 250 for the divided and the undivided cell configurations, respectively. The Faraday

https://doi.org/10.1021/acs.est.4c05481
Environ. Sci. Technol. 2024, 58, 14042−14051

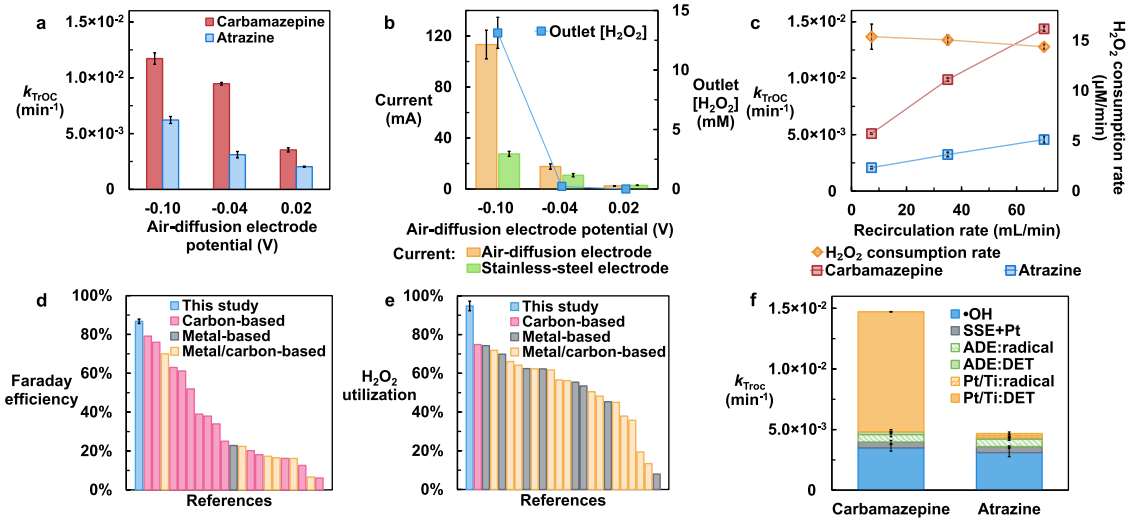

Figure 2. Removal of trace organic contaminants by the dual-cathode treatment system. Effect of applied potential on the air-diffusion electrode on: (a) removal rates of TrOCs and (b) currents and H_2O_2 concentrations at the outlet of the stainless-steel electrode. Effect of recirculation rate on (c) removal rates of TrOCs and H_2O_2 consumption rates by the stainless-steel electrode reactor. (d) Comparison of Faraday efficiency for H_2O_2 generation. The Faraday efficiency values used for this comparison were adapted from values measured in the absence of H_2O_2 activation catalysts. References were organized by the types of catalysts used for H_2O_2 generation. (e) Comparison of H_2O_2 utilization efficiency. References were organized by the types of catalysts used for H_2O_2 activation. (f) Removal pathways of carbamazepine and atrazine in the dual-cathode treatment system. SSE represents stainless-steel electrode; ADE represents air-diffusion electrode; DET represents direct electron transfer. Experimental conditions: 250 mM Na_2SO_4 buffered with 5 mM (a, b) or 1 mM (c) of PIPES buffer (pH 7), $[TrOCs]_0$ = 20 μg/L, applied current on air-diffusion electrode = 16 mA (c, f), applied potential on stainless-steel electrode = +0.02 V for all experiments. Recirculation rate = 35 mL/min (a, b) or 70 mL/min (f). Details of experiment depicted in Figure f are described in the Supporting Information. Data are presented as mean values with standard deviation. All potentials are reported versus SHE.

efficiency also increased from 21 to 87% for the divided configuration and from 9 to 64% for the undivided configuration. The produced H_2O_2 concentration is shown in Figure S8. The observed increase in the Faraday efficiency likely was due to an increase in the rate of the 2-electron reduction of O_2 (i.e., O_2 reduction to H_2O_2), relative to the rate of competing reactions (e.g., the 4-electron reduction of O_2 to H_2O). Because the air-diffusion electrode exhibited higher H_2O_2 production rates and higher Faraday efficiencies when a large applied overpotential was used, H_2O_2 generation likely benefited from the use of a high current density on the relatively small air-diffusion electrode. The long-term stability of the air-diffusion electrode was tested with an accelerated aging test (current density = 40 mA/cm^2). The electrode exhibited stable performance over 6 cycles of operation, with a total electrolysis time of 30 h (Figure S9).

Prevention of Unintended H_2O_2 Loss. In addition to activation to form $^{\cdot}OH$ on the stainless-steel electrode, H_2O_2 can be lost when the water encounters the anode through two different processes: (i) direct anodic oxidation (eq 2), and (ii) indirect anodic reactions, such as the oxidation of H_2O_2 by HOCl produced from anodic oxidation of Cl^- (eqs 3 and 4).

$$H_2O_2 \rightarrow 2H^+ + O_2 + 2e^- \quad (2)$$

$$Cl^- + H_2O \rightarrow H^+ + HOCl + 2e^- \quad (3)$$

$$H_2O_2 + HOCl \rightarrow H^+ + Cl^- + O_2 + H_2O \quad (4)$$

Separating the cathodic chamber from the anodic chamber by using a divided cell (no anodic flow into the cathode chamber, Figure S1) made it possible to avoid both decomposition pathways, resulting in a net increase of H_2O_2 production rate and increased the Faraday efficiency by a factor of 2.8 and 1.7, respectively (Figure 1b).

To determine the relative importance of direct and indirect oxidation of H_2O_2 on the anode, experiments were conducted in a chloride-free solution (i.e., 250 mM of Na_2SO_4 electrolyte containing less than 0.01 mM of chloride impurity) using divided and undivided reactors (Figure 1c). The Faraday efficiency observed in the Na_2SO_4 electrolyte was within 5% of the value observed in the authentic surface water, indicating that the presence of Cl^- at concentrations typical of freshwater (i.e., 10 mg/L = 0.28 mM) did not result in substantial loss of H_2O_2. In addition, H_2O_2 loss through direct oxidation, assessed by measuring H_2O_2 loss on the anode, was estimated to be responsible for an approximately 20% decrease in Faraday efficiency, which further confirmed that direct anodic oxidation of H_2O_2 was responsible for most of the observed differences in Faraday efficiency between the divided and undivided cells (Text S3 and Figure S10).

Although the divided cell configuration minimized H_2O_2 loss, sending water from the air-diffusion electrode chamber directly to the second (i.e., stainless-steel) cathode was not conducive to contaminant oxidation because the relatively high pH of water leaving the first cathode (Figure S11), which decreased the efficiency of conversion of H_2O_2 into $^{\cdot}OH$.[24] Because anodically formed HOCl resulted in a relatively small loss of H_2O_2 and acid production in the anode lowered the pH to values that were conducive to contaminant transformation,[24,42] a semidivided configuration was employed with the air-diffusion cathode placed between the Pt/Ti anode and the stainless-steel cathode (Figure 1d). A Pt mesh was placed downstream of the stainless-steel electrode to serve as the counter electrode for the stainless-steel cathode. Under the semidivided configuration, the water sequentially flowed through the Pt/Ti anode, air-diffusion cathode, stainless-steel cathode, and finally the Pt counter electrode (a detailed

https://doi.org/10.1021/acs.est.4c05481
Environ. Sci. Technol. 2024, 58, 14042−14051

schematic diagram for the experimental system is shown in Figure S12). When H_2O_2 generation and its activation were optimized, the stainless-steel electrode should have consumed all the produced H_2O_2, leaving no H_2O_2 to be oxidized by the Pt electrode. In this configuration, the pH values varied by less than 0.3 pH units as water passed between the different cell compartments, with the greatest change (about 0.5 pH units) observed in the effluent of the air-diffusion cathode when authentic surface water underwent treatment. Pt and Pt/Ti electrodes were used as counter electrodes in our experiments to assess processes taking place on the stainless-steel electrodes because of their low tendency to produce reactive species (e.g., $^{\cdot}OH$).[43] In an actual treatment module, it might be advantageous to replace the Pt and Pt/Ti electrodes with low-cost carbonaceous electrodes that could contribute to contaminant removal by direct oxidation.[44,45] The use of a shared anode that paired with both cathodes could be another improvement that would reduce the complexity of the current prototype.[46,47]

Trace Organic Contaminant Removal by a Combined Dual-Cathode Treatment System. The performance of the treatment train consisting of an air-diffusion electrode operated in series with a Pt/Ti electrode followed by a stainless-steel electrode was evaluated under various applied potentials using carbamazepine and atrazine as representative uncharged trace organic contaminants. When the stainless-steel electrode was operated at +0.02 V vs SHE, the potential found to be most efficient in conversion of H_2O_2 into $^{\cdot}OH$,[24,32] the rate of removal of the contaminants increased as the potential of the air-diffusion cathode decreased from +0.02 to −0.10 V vs SHE (Figure 2a).

The observed increase in contaminant transformation rates may have been due to an increase in the rate of H_2O_2 generation. Electron balance was conducted based on the Faraday efficiency for H_2O_2 generation (moles of H_2O_2 produced per two moles of electrons) and the electron utilization efficiency for H_2O_2 activation (62% at pH 7, meaning that 0.62 mol of H_2O_2 was transformed per mole of electrons consumed on the stainless-steel electrode).[24] We estimated that the optimal current ratio between the air-diffusion electrode to stainless-steel electrode for ensuring complete activation of H_2O_2 was 1.4, 2.1, and 5.9 for air-diffusion electrode operated at potentials of −0.10, −0.04, and +0.02 V vs SHE, respectively. Under these conditions, the observed current ratio was 4.1, 1.6, and 0.9 for those three potentials. The H_2O_2 produced on the air-diffusion electrode was not entirely activated by the stainless-steel electrode when a large overpotential was applied (i.e., $[H_2O_2]$ = 13 mM in water flowing out of the stainless-steel electrode when a potential of −0.10 V vs SHE was used), whereas all the H_2O_2 was depleted when highest potential (i.e., +0.02 V vs SHE) was applied to the air-diffusion electrode (Figure 2b). Because of the excess production of H_2O_2 at −0.10 V vs SHE and the higher H_2O_2 production rate at lower potentials, potentials lower than −0.10 V vs SHE for the air-diffusion electrode were expected to further lower the H_2O_2 utilization and thus were not studied. By adjusting the potential on the two electrodes separately (i.e., applying −0.04 V vs SHE on the air-diffusion electrode and +0.02 V vs SHE on the stainless-steel electrode) it was possible to balance the production of H_2O_2 with its activation to achieve removal of the contaminants without producing excess H_2O_2.

To assess the importance of mass transfer to contaminant removal, experiments were conducted with a constant current (i.e., 16 mA) on the air-diffusion electrode (current density = 1 mA/cm^2, applied potential around −0.04 V vs SHE). Increasing the recirculation rate from approximately 5 to 70 mL/min approximately tripled the rate of removal of the contaminants with minimal impact on the H_2O_2 consumption rate or the current ratio between the two electrodes (Figures 2c and S13). Therefore, we conclude that the increased rate of contaminant removal was caused by the enhanced mass transport of TrOCs to the electrode surface rather than more efficient activation of H_2O_2. This means that the flow-through mode overcame the mass-transport limitation of H_2O_2 to the electrode surface, which was previously identified as the rate-limiting step under batch mode operating conditions.[24]

Relative to composite electrodes employed for electrochemical advanced oxidation (Table S2), the dual-cathode treatment system demonstrated superior performance in terms of its ability to generate H_2O_2 (Figure 2d). The Faraday efficiency reported for composite electrodes are lower than the values reported for similar catalysts in well-controlled systems that are designed solely for H_2O_2 production.[48−50] The inferior performance is likely due to slow mass transport of O_2, unfavorable applied potentials necessitated by H_2O_2 activation, and the coating of the catalysts for H_2O_2 activation, which decreases the performance of H_2O_2 production by altering the electrode structure and affinity for O_2 interaction.[11,51,52]

Under the optimal conditions (−0.04 V vs SHE applied to the air-diffusion electrode and +0.02 V vs SHE applied to the stainless-steel electrode), the H_2O_2 transformed on the stainless-steel electrode was calculated to be 3.5 mM based on the H_2O_2 consumption rate, which accounted for 95% of the H_2O_2 produced by the air-diffusion electrode. The utilization efficiency of the produced H_2O_2 by the dual-cathode system was much higher than that observed on composite electrodes because of the optimal coupling between H_2O_2 production and activation (Figure 2e and Table S3).

The removal pathways for the two TrOCs were deconvoluted using probe compounds as described in Text S4 assuming that the reactive species that can oxidize methanol, 2-propanol, and dimethyl sulfoxide can be referred to as $^{\cdot}OH$ without differentiating between $^{\cdot}OH$ adsorbed on the electrode surface or $^{\cdot}OH$ reacting in the solution.[24,32] The $^{\cdot}OH$ pathway contributed to about 25% of the carbamazepine removal and 70% of the atrazine removal (Figure 2f). Direct electron transfer of carbamazepine on the Pt/Ti anodes contributed to about 70% of its removal.

The competition between the dissolved species and reductive species on the electrode surface (e.g., $\equiv$Fe(II) or e^-) for reacting with $^{\cdot}OH$ could result in surface scavenging of $^{\cdot}OH$, which controls the fate of $^{\cdot}OH$ and decreases the treatment performance of cathodic activation of H_2O_2 under batch-mode operation.[24] At a recirculation rate of 70 mL/min, the rate constant for reaction between $^{\cdot}OH$ and electrode surface was estimated as 2.4×10^3 cm^{-2} s^{-1} (Text S5), which corresponds to only about 30% of the values observed in the batch operation mode.[24] These results suggest that the enhanced mass transport under flow-through operating conditions decreased scavenging by the electrode surface, likely because of elevated concentrations of solutes near the surface that competed with the $^{\cdot}OH$ loss processes taking place on the electrode.

https://doi.org/10.1021/acs.est.4c05481
Environ. Sci. Technol. 2024, 58, 14042−14051

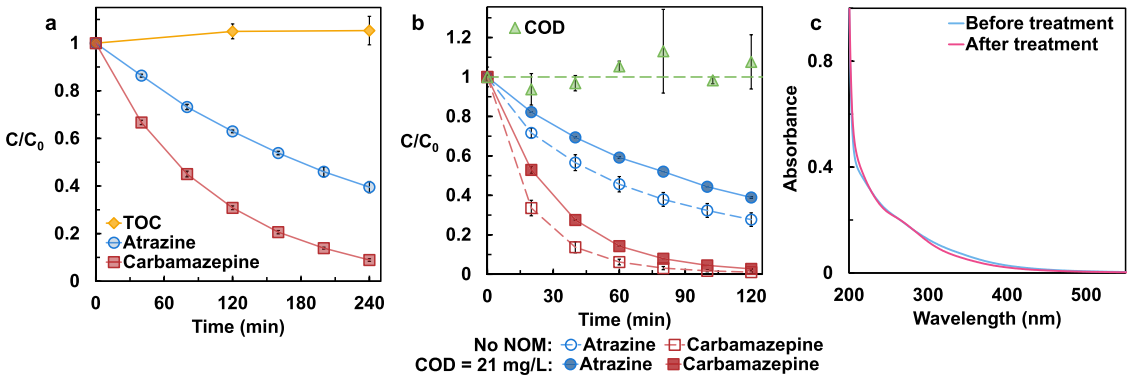

Figure 3. Selective oxidation of trace organic contaminants in the presence of natural organic matter. (a) Concentrations of TrOCs and TOC observed when authentic water was treated in the dual-cathode system, $[TOC]_0$ = 5.1 mg-C/L. (b) Concentrations of TrOCs and COD when a phosphate-buffered electrolyte was treated ($[PO_4^{3-}]$ = 2 mM, $[Na_2SO_4]$ = 250 mM, pH = 7), $[NOM]_0$ = 5.0 mg-C/L, $[COD]_0$ = 21 mg/L. The interference of H_2O_2 on COD measurement was corrected based on concentration of H_2O_2 in each sample. (c) UV−vis absorption spectrum of the NOM-containing electrolyte before and after 2 h of treatment. Data are presented as mean values with standard deviation.

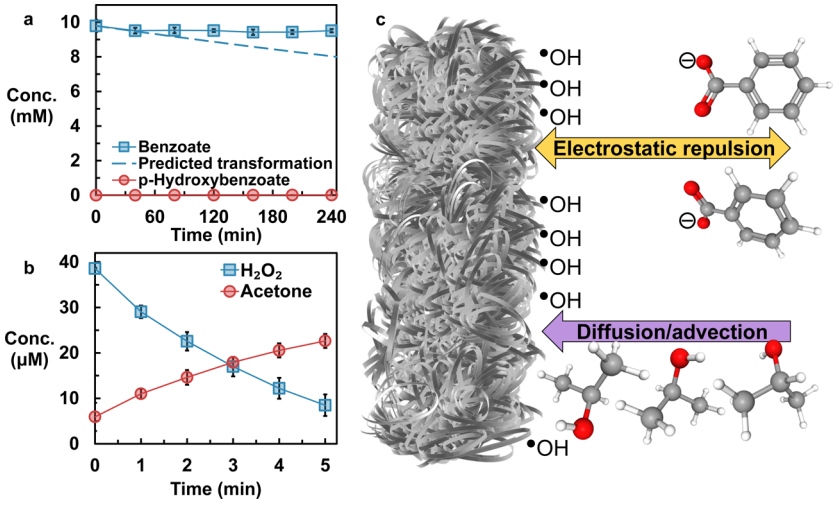

Figure 4. ·OH scavenged by ·OH scavengers of different charges. (a) Transformation and formation of oxidation products during treatment of 10 mM benzoate. Conditions: 250 mM Na_2SO_4 buffered with 1 mM of PIPES buffer (pH 7), applied current on air-diffusion electrode = 16 mA, applied potential on stainless-steel electrode = +0.02 V vs SHE, recirculation rate = 70 mL/min. (b) Formation of acetone from oxidation of 2-propanol by ·OH produced on the stainless-steel electrode. Experiments conducted in a divided H-type reactor to prevent oxidation of 2-propanol on the anodes, 200 mM Na_2SO_4 buffered with 1 mM PIPES (pH 7), $[2\text{-propanol}]_0$ = 100 mM, $[H_2O_2]_0$ = 37 μM, applied potential on stainless-steel electrode = +0.02 V vs SHE. (c) Schematic illustration of electrostatic repulsion of negatively charged ·OH scavengers by the electrode surface. Data are presented as mean values with standard deviation.

Removal of Trace Organic Contaminants from Authentic Surface Water. The performance of the dual-cathode treatment system under realistic operating conditions was assessed in an authentic surface water sample containing 5.1 mg-C/L of NOM (without addition of supporting electrolytes or buffers). Carbamazepine and atrazine were used as representative uncharged contaminants because of their high frequencies of detection in nontraditional water sources.[53−55] Over the course of 4 h, the dual-cathode treatment system removed more than 90% of the carbamazepine and 60% of the atrazine. In contrast, the total organic carbon (TOC) concentration, which mainly consisted of NOM, remained unchanged (Figure 3a). The effect of NOM was also assessed in an electrolyte with and without 5.0 mg-C/L of Suwannee River NOM (Figure 3b). The chemical oxygen demand (COD) remained almost constant throughout the treatment and the transformation rates of TrOCs decreased by less than 25% when NOM was added. For comparison, addition of 5.0 mg-C/L of NOM would decrease the transformation rates of TrOCs in a homogeneous ·OH-based advanced oxidation process by about a factor of 10, assuming addition of NOM had no impact on the formation of ·OH (Text S6). Furthermore, the UV−vis absorption spectrum of the water did not change appreciably during treatment (Figure 3c).[56] Therefore, we conclude that the dual-cathode treatment system selectively oxidizes TrOCs without oxidizing NOM. The slight decline in removal efficiency in the presence of NOM was likely due to inhibition of contaminant transformation by non-·OH pathways (e.g., direct electron transfer on the anodes, Figure 2f). The concentrations of Fe and Cr released during the treatment of the authentic surface water remained below the drinking water standards throughout the experiment (Figure S15).[57,58]

Electrostatic Repulsion of Negatively Charged ·OH Scavengers. To elucidate the mechanisms of selective oxidation of TrOCs in the presence of NOM, a negatively charged compound (benzoate) and an uncharged compound (2-propanol) were employed as radical scavengers. Under

https://doi.org/10.1021/acs.est.4c05481
Environ. Sci. Technol. 2024, 58, 14042−14051

conditions used in these experiments, we predicted that approximately 20% of either compound would be removed by ·OH produced on the stainless-steel electrode over the course of the experiment (Text S7). However, benzoate concentrations remained close to their initial values throughout the experiment and only around 10 μM of the most prominent benzoate transformation product (para-hydroxybenzoate), an amount corresponding to approximately 0.1% of $[benzoate]_0$, was detected (Figure 4a). An experiment in which trace concentrations of carbamazepine and atrazine were oxidized in the presence of a high concentration of benzoate (i.e., 10 mM) indicated that benzoate did not affect the rate of transformation of uncharged organic contaminants by scavenging ·OH (Figure S16). These results indicated that the negatively charge compound (benzoate) did not interact to an appreciable degree with ·OH produced in the dual-cathode treatment system.

In contrast, approximately 90% of the neutral radical scavenger (2-propanol) was transformed in an experiment conducted under the same conditions (Figure S17). Because some of the 2-propanol could have been oxidized by the anodes,[59] the oxidation of 2-propanol by ·OH produced on the stainless-steel electrode was confirmed using a divided H-type reactor in which the anodic processes were eliminated (Figure 4b). Furthermore, the observed reduction in the rate of oxidation of atrazine in the presence of 10 and 200 mM 2-propanol was consistent with predictions assuming 2-propanol scavenged ·OH produced on the stainless-steel electrode (Figure S16). Therefore, the ·OH produced from H_2O_2 activation on the stainless-steel electrode was scavenged by a neutral organic compound (2-propanol) but not by a charged compound (benzoate).

The difference between the behavior of 2-propanol and benzoate most likely was due to electrostatic repulsion between the negatively charged cathode surface and the negatively charged benzoate, which resulted in locally lower benzoate concentration near the electrode surface where the ·OH was being produced. The diffusion distance of ·OH in the aqueous phase, estimated from the Einstein−Smoluchowski equation, was around 8 nm (Text S8),[60] which was about 3 orders of magnitude smaller than the local concentration gradients of charged species (i.e., negatively charged species like benzoate could be repelled by tens of micrometers from the electrode surface).[61−64] Therefore, the dual-cathode treatment system exhibited selective oxidation of uncharged compounds in the presence of charged compounds like NOM due to electrostatic repulsion of negatively charged ·OH scavengers (Figure 4c).

Application Potential and Engineering Considerations. One of the main challenges in the application of electrochemical techniques to drinking water treatment is the low conductivity of freshwater, which results in a high ohmic loss between the working electrodes and counter electrodes. For the treatment of low conductivity surface water (i.e., 75 mg/L total dissolved solids, conductivity = 255 μS/cm), the electrical energy per order values were determined as 4.2 ± 0.3 kWh/m^3 for carbamazepine and 11.1 ± 1.4 kWh/m^3 for atrazine,[65] with about 90% of the energy consumed by the air-diffusion electrode (Figure 5). Assuming a person needs 10 L/day of clean drinking water, the energy consumption would be approximately 0.1 kWh/capita/day. This energy consumption of the dual-cathode treatment system is comparable to that of

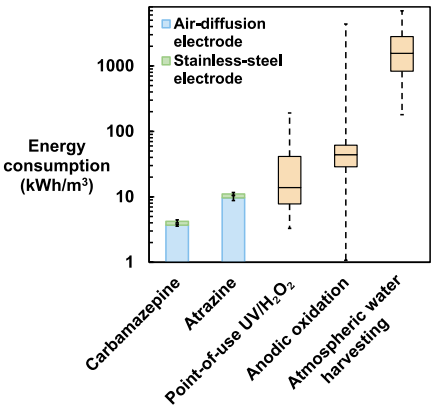

Figure 5. Comparison of the energy consumption of the dual-cathode treatment system with other technologies. The values for the dual-cathode treatment system were calculated based on the treatment of the authentic surface water. The energy consumption was reported for 90% reduction of contaminants (i.e., electrical energy per order) except for atmospheric water harvesting. Data are presented as mean values with standard deviation. Box plot represents data as median with 25/75 percentile (box) and minimum−maximum (whiskers).

other distributed drinking water treatment technologies (Text S9 and Tables S4 and S5).[66−68] Because the air-diffusion electrode consumed about 90% of the total energy, further improvements should focus on reducing the interelectrode distance of the air-diffusion electrode reactor by using thinner plastic frames and gaskets.

Because the transformation of contaminants by ·OH takes place near the surface of the stainless-steel electrodes, the performance of the up-scaled prototypes could be simulated using the removal rates depicted in Figure 2f with an assumption that the transformation rate of reactions involving ·OH is proportional to the ratio of stainless-steel surface area to the solution volume (Text S10). Operation of the stainless-steel electrode as a single-pass flow-through reactor is expected to significantly increase the rate of removal of contaminants because flow-through reactors do not have large void volumes like those employed in the laboratory-scale recirculating system (e.g., the Erlenmeyer flasks depicted in Figure S12). In other words, all the water in a flow-through reactor will pass through the stainless-steel electrode, whereas less than 25% of the water was in contact with the stainless-steel cathode in the recirculating system used in these experiments. Further improvements to the performance of the flow-through system might be achieved by decreasing the porosity of the stainless-steel electrode or increasing its specific surface area (porosity = 0.95, specific surface area = 80 cm^2/g for the current stainless-steel electrode, Figure S18). For example, we predict that 90% removal of atrazine could be achieved with a 3 min hydraulic residence time using a compact stainless-steel frit reactor (volume of stainless-steel frit = 90 mL, porosity = 0.47, specific surface area = 240 cm^2/g, McMaster-Carr, Figure S19) coupled to an air-diffusion electrode of 8.5 cm × 8.5 cm.

Environmental Implications. Electrified water treatment provides a suitable approach to treat nontraditional waters at remote locations because of their ability to generate chemical reagents in situ. This approach offers major advantages over dual-functional catalysts in which performance is limited by the slow mass transport of O_2 or contaminants and ineffective utilization of the produced H_2O_2. Separating the H_2O_2 generation and activation steps by using two separate

https://doi.org/10.1021/acs.est.4c05481
Environ. Sci. Technol. 2024, 58, 14042−14051

electrodes provides greater efficiency and more easily controlled operations. The dual-cathode treatment system demonstrated a superior performance with respect to H_2O_2 production and utilization and produced H_2O_2-free treated water.

In contrast to the previously developed systems that often rely upon exotic nanomaterials as catalysts,[31] the dual-cathode treatment systems used inexpensive materials as catalysts. The cost of an 8 cm × 8 cm air-diffusion electrode was estimated to be less than $6 (Table S6), and the cost of a 20 g stainless-steel electrode costs was estimated to be less than $1. These low costs should make these systems cost-competitive for point-of-use and point-of-entry water treatment applications.

The interference of NOM on the transformation of TrOCs has hindered the application of ·OH-based advanced oxidation processes due to their lack of selectivity.[16] Previous efforts to mitigate interference by NOM have attempted to employ size exclusion to separate NOM from the target contaminants.[69] However, size exclusion of NOM often requires a relatively small pore size (e.g., <20 nm), which can be clogged by bubbles generated from electrochemical reactions and therefore is difficult to use with electrochemical processes.[70] In this study, we demonstrated that NOM could be separated from neutral contaminants by electrostatic repulsion, which prevented the quenching of ·OH by NOM. Although electrostatic repulsion may hinder the removal of negatively charged contaminants, other electrochemical processes can be integrated into the treatment system to remove those contaminants (e.g., the user could replace the relatively inert Pt anode with anodes that exhibit high reactivity toward contaminant transformation).[71] The selective oxidation of contaminants highlighted a major advantage of cathodic advanced oxidation processes over the conventional anodic advanced oxidation processes, in which the electrostatic attraction of NOM has often been viewed as a parasitic and detrimental process.

■ ASSOCIATED CONTENT

Supporting Information

The Supporting Information is available free of charge at https://pubs.acs.org/doi/10.1021/acs.est.4c05481.

Details about equilibrium potential calculation, water quality parameters, reactor schematic, analytical methods, H_2O_2 anodic decomposition, trace organic contaminant transformation pathways, ·OH scavenging by stainless-steel electrode, predicted ·OH scavenging by natural organic matter, metal released from stainless-steel electrode, transformation of ·OH scavengers, calculation of diffusion distance of ·OH, energy consumption and cost analysis, scale-up analysis (PDF)

■ AUTHOR INFORMATION

Corresponding Author

David L. Sedlak − *Department of Civil & Environmental Engineering, University of California, Berkeley, Berkeley, California 94720, United States;* orcid.org/0000-0003-1686-8464; Email: sedlak@berkeley.edu

Author

Yanghua Duan − *Department of Civil & Environmental Engineering, University of California, Berkeley, Berkeley, California 94720, United States;* orcid.org/0000-0003-2587-1278

Complete contact information is available at: https://pubs.acs.org/10.1021/acs.est.4c05481

Notes

The authors declare no competing financial interest.

■ ACKNOWLEDGMENTS

This material is based upon work supported by the National Alliance for Water Innovation (NAWI), funded by the U.S. Department of Energy, Energy Efficiency and Renewable Energy Office, Advanced Manufacturing Office under Funding Opportunity Announcement DE-FOA-0001905 and funded in part through agreement No. D2105001 with the California State Water Resources Control Board to the Regents of the University of California, Office of the President using funds from Proposition 1.

■ REFERENCES

(1) Radjenovic, J.; Sedlak, D. L. Challenges and Opportunities for Electrochemical Processes as Next-Generation Technologies for the Treatment of Contaminated Water. *Environ. Sci. Technol.* **2015**, *49* (19), 11292−11302.

(2) von Gunten, U. Oxidation processes in water treatment: are we on track? *Environ. Sci. Technol.* **2018**, *52* (9), 5062−5075.

(3) Dhanda, N.; Panday, Y. K.; Kumar, S. Recent advances in the electrochemical production of hydrogen peroxide. *Electrochim. Acta* **2024**, *481*, No. 143872.

(4) Shen, X.; Xiao, F.; Zhao, H.; Chen, Y.; Fang, C.; Xiao, R.; Chu, W.; Zhao, G. In Situ-Formed PdFe Nanoalloy and Carbon Defects in Cathode for Synergic Reduction−Oxidation of Chlorinated Pollutants in Electro-Fenton Process. *Environ. Sci. Technol.* **2020**, *54* (7), 4564−4572.

(5) Ganiyu, S. O.; Zhou, M.; Martínez-Huitle, C. A. Heterogeneous electro-Fenton and photoelectro-Fenton processes: A critical review of fundamental principles and application for water/wastewater treatment. *Applied Catalysis B: Environmental* **2018**, *235*, 103−129.

(6) Zhao, K.; Quan, X.; Su, Y.; Qin, X.; Chen, S.; Yu, H. Enhanced Chlorinated Pollutant Degradation by the Synergistic Effect between Dechlorination and Hydroxyl Radical Oxidation on a Bimetallic Single-Atom Catalyst. *Environ. Sci. Technol.* **2021**, *55* (20), 14194−14203.

(7) Liu, K.; Yu, J. C.-C.; Dong, H.; Wu, J. C. S.; Hoffmann, M. R. Degradation and Mineralization of Carbamazepine Using an Electro-Fenton Reaction Catalyzed by Magnetite Nanoparticles Fixed on an Electrocatalytic Carbon Fiber Textile Cathode. *Environ. Sci. Technol.* **2018**, *52* (21), 12667−12674.

(8) Cao, P.; Quan, X.; Zhao, K.; Chen, S.; Yu, H.; Su, Y. High-Efficiency Electrocatalysis of Molecular Oxygen toward Hydroxyl Radicals Enabled by an Atomically Dispersed Iron Catalyst. *Environ. Sci. Technol.* **2020**, *54* (19), 12662−12672.

(9) Li, Y.; Miller, C. J.; Wu, L.; Waite, T. D. Hydroxyl Radical Production via a Reaction of Electrochemically Generated Hydrogen Peroxide and Atomic Hydrogen: An Effective Process for Contaminant Oxidation? *Environ. Sci. Technol.* **2022**, *56* (9), 5820−5829.

(10) Li, J.; Ai, Z.; Zhang, L. Design of a neutral electro-Fenton system with Fe@Fe_2O_3/ACF composite cathode for wastewater treatment. *Journal of Hazardous Materials* **2009**, *164* (1), 18−25.

(11) Liu, F.; Liu, Y.; Yao, Q.; Wang, Y.; Fang, X.; Shen, C.; Li, F.; Huang, M.; Wang, Z.; Sand, W.; Xie, J. Supported Atomically-Precise Gold Nanoclusters for Enhanced Flow-through Electro-Fenton. *Environ. Sci. Technol.* **2020**, *54* (9), 5913−5921.

(12) Wang, C.; Gu, Y.; Wu, S.; Yu, H.; Chen, S.; Su, Y.; Guo, Y.; Wang, X.; Chen, H.; Kang, W.; Quan, X. Construction of a Microchannel Electrochemical Reactor with a Monolithic Porous-

Carbon Cathode for Adsorption and Degradation of Organic Pollutants in Several Minutes of Retention Time. *Environ. Sci. Technol.* **2020**, *54* (3), 1920−1928.
(13) Jiang, W.-L.; Xia, X.; Han, J.-L.; Ding, Y.-C.; Haider, M. R.; Wang, A.-J. Graphene Modified Electro-Fenton Catalytic Membrane for in Situ Degradation of Antibiotic Florfenicol. *Environ. Sci. Technol.* **2018**, *52* (17), 9972−9982.
(14) Guo, D.; Liu, Y.; Ji, H.; Wang, C.-C.; Chen, B.; Shen, C.; Li, F.; Wang, Y.; Lu, P.; Liu, W. Silicate-Enhanced Heterogeneous Flow-Through Electro-Fenton System Using Iron Oxides under Nano-confinement. *Environ. Sci. Technol.* **2021**, *55* (6), 4045−4053.
(15) Gao, G.; Zhang, Q.; Hao, Z.; Vecitis, C. D. Carbon Nanotube Membrane Stack for Flow-through Sequential Regenerative Electro-Fenton. *Environ. Sci. Technol.* **2015**, *49* (4), 2375−2383.
(16) Duan, Y.; Sedlak, D. L. An electrochemical advanced oxidation process for the treatment of urban stormwater. *Water Research X* **2021**, *13*, No. 100127.
(17) Barazesh, J. M.; Hennebel, T.; Jasper, J. T.; Sedlak, D. L. Modular Advanced Oxidation Process Enabled by Cathodic Hydrogen Peroxide Production. *Environ. Sci. Technol.* **2015**, *49* (12), 7391−7399.
(18) Valim, R. B.; Reis, R. M.; Castro, P. S.; Lima, A. S.; Rocha, R. S.; Bertotti, M.; Lanza, M. R. V. Electrogeneration of hydrogen peroxide in gas diffusion electrodes modified with tert-butylanthraquinone on carbon black support. *Carbon* **2013**, *61*, 236−244.
(19) Zhang, Q.; Zhou, M.; Ren, G.; Li, Y.; Li, Y.; Du, X. Highly efficient electrosynthesis of hydrogen peroxide on a superhydrophobic three-phase interface by natural air diffusion. *Nat. Commun.* **2020**, *11* (1), 1731.
(20) Casado, J. Towards industrial implementation of Electro-Fenton and derived technologies for wastewater treatment: A review. *Journal of Environmental. Chemical Engineering* **2019**, *7* (1), No. 102823.
(21) Zhang, Y.; Wang, Y.; Angelidaki, I. Alternate switching between microbial fuel cell and microbial electrolysis cell operation as a new method to control H_2O_2 level in Bioelectro-Fenton system. *J. Power Sources* **2015**, *291*, 108−116.
(22) Song, Y.; Wang, A.; Ren, S.; Zhang, Y.; Wen, Z.; Zhang, Z. A novel sandwich structure ACF/CC@FeOCl as bifunctional cathode for efficient mineralization of trimethoprim in the heterogeneous electro-Fenton process over a wide pH range. *J. Chem. Technol. Biotechnol.* **2022**, *97* (12), 3333−3343.
(23) Ting, W.-P.; Lu, M.-C.; Huang, Y.-H. The reactor design and comparison of Fenton, electro-Fenton and photoelectro-Fenton processes for mineralization of benzene sulfonic acid (BSA). *Journal of Hazardous Materials* **2008**, *156* (1), 421−427.
(24) Duan, Y.; Jiang, W.; Sedlak, D. L. Surface Processes Control the Fate of Reactive Oxidants Generated by Electrochemical Activation of Hydrogen Peroxide on Stainless-Steel Electrodes. *Environ. Sci. Technol.* **2023**, *57* (47), 18680−18689.
(25) Zhang, Q.; Zhou, M.; Du, X.; Su, P.; Fu, W.; Song, G. Highly efficient dual-cathode Electro-Fenton process without aeration at a wide pH range: Simultaneously enhancing Fe(II) regeneration and mineralization efficiency. *Chemical Engineering Journal* **2022**, *429*, No. 132436.
(26) Wang, D.; Hu, J.; Liu, B.; Hou, H.; Yang, J.; Li, Y.; Zhu, Y.; Liang, S.; Xiao, K. Degradation of refractory organics in dual-cathode electro-Fenton using air-cathode for H_2O_2 electrogeneration and microbial fuel cell cathode for Fe^{2+} regeneration. *Journal of Hazardous Materials* **2021**, *412*, No. 125269.
(27) Deng, F.; Li, S.; Cao, Y.; Fang, M. A.; Qu, J.; Chen, Z.; Qiu, S. A dual-cathode pulsed current electro-Fenton system: Improvement for H_2O_2 accumulation and Fe^{3+} reduction. *J. Power Sources* **2020**, *466*, No. 228342.
(28) Cui, L.; Sun, M.; Zhang, Z. An efficient, green, and residual oxidant-free wastewater treatment technique enabled by coupling a dual-cathode heterogeneous electro-Fenton process and UV radiation in tandem. *Green Chem.* **2023**, *25* (16), 6315−6326.
(29) Chu, Y. Y.; Qian, Y.; Wang, W. J.; Deng, X. L. A dual-cathode electro-Fenton oxidation coupled with anodic oxidation system used for 4-nitrophenol degradation. *Journal of Hazardous Materials* **2012**, *199*−*200*, 179−185.
(30) Chu, Y.; Wang, J.; Lv, R. Degradation of 2,4-Dichlorophenol Solution and Toxicity Reduction by a Dual-Cathode Oxidation System. *Environmental Engineering Science* **2016**, *33* (8), 544−550.
(31) Wang, J.; Li, S.; Qin, Q.; Peng, C. Sustainable and feasible reagent-free electro-Fenton via sequential dual-cathode electrocatalysis. *Proc. Natl. Acad. Sci. U. S. A.* **2021**, *118* (34), No. e2108573118.
(32) Weng, C.; Chuang, Y.-H.; Davey, B.; Mitch, W. A. Reductive Electrochemical Activation of Hydrogen Peroxide as an Advanced Oxidation Process for Treatment of Reverse Osmosis Permeate during Potable Reuse. *Environ. Sci. Technol.* **2020**, *54* (19), 12593−12601.
(33) Stirling, R.; Walker, W. S.; Westerhoff, P.; Garcia-Segura, S. Techno-economic analysis to identify key innovations required for electrochemical oxidation as point-of-use treatment systems. *Electrochim. Acta* **2020**, *338*, No. 135874.
(34) Atrashkevich, A.; Garcia-Segura, S. Navigating the electro-disinfection frontier: A roadmap towards resilient implementation. *Current Opinion in Electrochemistry* **2024**, *43*, No. 101437.
(35) Eisenberg, G. Colorimetric determination of hydrogen peroxide. *Industrial & Engineering Chemistry Analytical Edition* **1943**, *15* (5), 327−328.
(36) Bader, H.; Sturzenegger, V.; Hoigné, J. Photometric method for the determination of low concentrations of hydrogen peroxide by the peroxidase catalyzed oxidation of N,N-diethyl-p-phenylenediamine (DPD). *Water Res.* **1988**, *22* (9), 1109−1115.
(37) Tsou, K.; Antell, E.; Duan, Y.; Olivares, C. I.; Yi, S.; Alvarez-Cohen, L.; Sedlak, D. L. Improved Total Oxidizable Precursor Assay for Quantifying Polyfluorinated Compounds Amenable to Oxidative Conversion to Perfluoroalkyl Carboxylic Acids. *ACS ES&T Water* **2023**, *3* (9), 2996−3003.
(38) Kim, H. W.; Ross, M. B.; Kornienko, N.; Zhang, L.; Guo, J.; Yang, P.; McCloskey, B. D. Efficient hydrogen peroxide generation using reduced graphene oxide-based oxygen reduction electrocatalysts. *Nature Catalysis* **2018**, *1* (4), 282−290.
(39) Liang, J.; Wang, Y.; Liu, Q.; Luo, Y.; Li, T.; Zhao, H.; Lu, S.; Zhang, F.; Asiri, A. M.; Liu, F.; Ma, D.; Sun, X. Electrocatalytic hydrogen peroxide production in acidic media enabled by NiS_2 nanosheets. *Journal of Materials Chemistry A* **2021**, *9* (10), 6117−6122.
(40) Sheng, H.; Hermes, E. D.; Yang, X.; Ying, D.; Janes, A. N.; Li, W.; Schmidt, J. R.; Jin, S. Electrocatalytic Production of H_2O_2 by Selective Oxygen Reduction Using Earth-Abundant Cobalt Pyrite (CoS_2). *ACS Catal.* **2019**, *9* (9), 8433−8442.
(41) Bormann, S.; van Schie, M. M. C. H.; De Almeida, T. P.; Zhang, W.; Stöckl, M.; Ulber, R.; Hollmann, F.; Holtmann, D. H_2O_2 Production at Low Overpotentials for Electroenzymatic Halogenation Reactions. *ChemSusChem* **2019**, *12* (21), 4759−4763.
(42) Lammers, L. N.; Duan, Y.; Anaya, L.; Koishi, A.; Lopez, R.; Delima, R.; Jassby, D.; Sedlak, D. L. Electrolytic Sulfuric Acid Production with Carbon Mineralization for Permanent Carbon Dioxide Removal. *ACS Sustainable Chem. Eng.* **2023**, *11* (12), 4800−4812.
(43) Chaplin, B. P. Critical review of electrochemical advanced oxidation processes for water treatment applications. *Environmental Science: Processes & Impacts* **2014**, *16* (6), 1182−1203.
(44) Duinslaeger, N.; Radjenovic, J. Electrochemical degradation of per- and polyfluoroalkyl substances (PFAS) using low-cost graphene sponge electrodes. *Water Res.* **2022**, *213*, No. 118148.
(45) Baptista-Pires, L.; Norra, G.-F.; Radjenovic, J. Graphene-based sponges for electrochemical degradation of persistent organic contaminants. *Water Res.* **2021**, *203*, No. 117492.
(46) Chu, N.; Jiang, Y.; Zhang, L.; Zeng, R. J.; Li, D. Biocathode prepared at low anodic potentials achieved a higher response for water

https://doi.org/10.1021/acs.est.4c05481
Environ. Sci. Technol. 2024, 58, 14042−14051

biotoxicity monitoring after polarity reversal. *Science of The Total Environment* **2022**, *847*, No. 157553.
(47) Atkinson, J. T.; Su, L.; Zhang, X.; Bennett, G. N.; Silberg, J. J.; Ajo-Franklin, C. M. Real-time bioelectronic sensing of environmental contaminants. *Nature* **2022**, *611* (7936), 548−553.
(48) Zhang, X.; Zhao, X.; Zhu, P.; Adler, Z.; Wu, Z.-Y.; Liu, Y.; Wang, H. Electrochemical oxygen reduction to hydrogen peroxide at practical rates in strong acidic media. *Nat. Commun.* **2022**, *13* (1), 2880.
(49) Xia, Y.; Zhao, X.; Xia, C.; Wu, Z.-Y.; Zhu, P.; Kim, J. Y.; Bai, X.; Gao, G.; Hu, Y.; Zhong, J.; Liu, Y.; Wang, H. Highly active and selective oxygen reduction to H_2O_2 on boron-doped carbon for high production rates. *Nat. Commun.* **2021**, *12* (1), 4225.
(50) Zhou, Y.; Chen, G.; Zhang, J. A review of advanced metal-free carbon catalysts for oxygen reduction reactions towards the selective generation of hydrogen peroxide. *Journal of Materials Chemistry A* **2020**, *8* (40), 20849−20869.
(51) Zhao, H.; Qian, L.; Guan, X.; Wu, D.; Zhao, G. Continuous Bulk FeCuC Aerogel with Ultradispersed Metal Nanoparticles: An Efficient 3D Heterogeneous Electro-Fenton Cathode over a Wide Range of pH 3−9. *Environ. Sci. Technol.* **2016**, *50* (10), 5225−5233.
(52) Wang, Y.; Zhao, G.; Chai, S.; Zhao, H.; Wang, Y. Three-Dimensional Homogeneous Ferrite-Carbon Aerogel: One Pot Fabrication and Enhanced Electro-Fenton Reactivity. *ACS Appl. Mater. Interfaces* **2013**, *5* (3), 842−852.
(53) Spahr, S.; Teixidó, M.; Sedlak, D. L.; Luthy, R. G. Hydrophilic trace organic contaminants in urban stormwater: occurrence, toxicological relevance, and the need to enhance green stormwater infrastructure. *Environmental Science: Water Research & Technology* **2020**, *6* (1), 15−44.
(54) Tixier, C.; Singer, H. P.; Oellers, S.; Müller, S. R. Occurrence and Fate of Carbamazepine, Clofibric Acid, Diclofenac, Ibuprofen, Ketoprofen, and Naproxen in Surface Waters. *Environ. Sci. Technol.* **2003**, *37* (6), 1061−1068.
(55) de Souza, R. M.; Seibert, D.; Quesada, H. B.; de Jesus Bassetti, F.; Fagundes-Klen, M. R.; Bergamasco, R. Occurrence, impacts and general aspects of pesticides in surface water: A review. *Process Safety and Environmental Protection* **2020**, *135*, 22−37.
(56) Wang, G. S.; Liao, C. H.; Chen, H. W.; Yang, H. C. Characteristics of Natural Organic Matter Degradation in Water by UV/H_2O_2 Treatment. *Environmental Technology* **2006**, *27* (3), 277−287.
(57) United States Environmental Protection Agency, *National primary drinking water regulations*; https://www.epa.gov/ground-water-and-drinking-water/national-primary-drinking-water-regulations. Accessed 11 Jan. 2023.
(58) United States Environmental Protection Agency, *Secondary Drinking Water Standards: Guidance for Nuisance Chemicals*; https://www.epa.gov/sdwa/secondary-drinking-water-standards-guidance-nuisance-chemicals. Accessed 11 Jan. 2023.
(59) Okanishi, T.; Katayama, Y.; Ito, R.; Muroyama, H.; Matsui, T.; Eguchi, K. Electrochemical oxidation of 2-propanol over platinum and palladium electrodes in alkaline media studied by in situ attenuated total reflection infrared spectroscopy. *Phys. Chem. Chem. Phys.* **2016**, *18* (15), 10109−10115.
(60) Schwarzenbach, R. P.; Gschwend, P. M.; Imboden, D. M. *Environmental organic chemistry*; John Wiley & Sons, 2005.
(61) Rudd, N. C.; Cannan, S.; Bitziou, E.; Ciani, I.; Whitworth, A. L.; Unwin, P. R. Fluorescence Confocal Laser Scanning Microscopy as a Probe of pH Gradients in Electrode Reactions and Surface Activity. *Anal. Chem.* **2005**, *77* (19), 6205−6217.
(62) Lu, X.; Zhu, C.; Wu, Z.; Xuan, J.; Francisco, J. S.; Wang, H. In Situ Observation of the pH Gradient near the Gas Diffusion Electrode of CO_2 Reduction in Alkaline Electrolyte. *J. Am. Chem. Soc.* **2020**, *142* (36), 15438−15444.
(63) Cannan, S.; Douglas Macklam, I.; Unwin, P. R. Three-dimensional imaging of proton gradients at microelectrode surfaces using confocal laser scanning microscopy. *Electrochem. Commun.* **2002**, *4* (11), 886−892.
(64) Auinger, M.; Katsounaros, I.; Meier, J. C.; Klemm, S. O.; Biedermann, P. U.; Topalov, A. A.; Rohwerder, M.; Mayrhofer, K. J. J. Near-surface ion distribution and buffer effects during electrochemical reactions. *Phys. Chem. Chem. Phys.* **2011**, *13* (36), 16384−16394.
(65) Bolton, J. R.; Bircher, K. G.; Tumas, W.; Tolman, C. A. Figures-of-merit for the technical development and application of advanced oxidation technologies for both electric- and solar-driven systems (IUPAC Technical Report). *Pure Appl. Chem.* **2001**, *73* (4), 627−637.
(66) Miklos, D. B.; Remy, C.; Jekel, M.; Linden, K. G.; Drewes, J. E.; Hubner, U. Evaluation of advanced oxidation processes for water and wastewater treatment - A critical review. *Water Res.* **2018**, *139*, 118−131.
(67) Bagheri, F. Performance investigation of atmospheric water harvesting systems. *Water Resources and Industry* **2018**, *20*, 23−28.
(68) Tu, R.; Hwang, Y. Reviews of atmospheric water harvesting technologies. *Energy* **2020**, *201*, No. 117630.
(69) Zhang, S.; Hedtke, T.; Zhu, Q.; Sun, M.; Weon, S.; Zhao, Y.; Stavitski, E.; Elimelech, M.; Kim, J.-H. Membrane-Confined Iron Oxychloride Nanocatalysts for Highly Efficient Heterogeneous Fenton Water Treatment. *Environ. Sci. Technol.* **2021**, *55* (13), 9266−9275.
(70) Darband, G. B.; Aliofkhazraei, M.; Shanmugam, S. Recent advances in methods and technologies for enhancing bubble detachment during electrochemical water splitting. *Renewable and Sustainable Energy Reviews* **2019**, *114*, No. 109300.
(71) Jiang, W.; Duan, Y.; Bandaru, S. R. S.; Radjenovic, J.; Sedlak, D. L.; Mi, B. Inhibition of chlorinated byproducts formation by boron-doped rGO electrodes during electrooxidation of trace organic contaminants. *Applied Catalysis B: Environment and Energy* **2024**, *357*, No. 124303.

https://doi.org/10.1021/acs.est.4c05481
Environ. Sci. Technol. 2024, 58, 14042−14051